ORIGINAL RESEARCH

Flower flake-shaped zinc oxide nanoparticles synthesized by microwave technique with different plant extracts for anti-bacterial activity

Article history:
Received: 21-02-2024
Revised: 04-10-2024
Accepted: 28-11-2024

Nirdosh Verma[a], Lacy Loveleen[b], Surendra Nimesh[c], Sunil Kumar[d], Kuldeep Kumar[e], Kamal Jeet[f], Naveen Thakur[g]

Abstract: Plants are recognized for containing crucial phytochemicals that play a significant role in reducing and capping nanoparticles, contributing to advancements in nanoparticle synthesis. The use of plant extracts as stabilizing agents in nanoparticle synthesis has gained immense popularity in contemporary research. These stabilizing agents also help mitigate the potential toxic effects of chemicals used in the synthesis process. In this study, four distinct plants-*Psidium guajava, Colocasia esculenta, Phyllanthus emblica,* and *Murraya koenigii* were selected as stabilizers for the synthesis of ZnO nanoparticles using the microwave technique. Various characterization techniques, including X-ray diffraction (XRD), scanning electron microscopy (SEM), energy-dispersive X-ray spectroscopy (EDX), transmission electron microscopy (TEM), UV-Vis spectroscopy, and Fourier-transform infrared spectroscopy (FTIR), were employed to elucidate the morphology, band gap, and functional groups of the synthesized nanoparticles. XRD analysis revealed crystallite sizes of 14 nm for *Psidium guajava,* 12 nm for *Colocasia esculenta,* 17 nm for *Phyllanthus emblica,* and 13 nm for *Murraya koenigii.* The corresponding band gaps were 3.28 eV, 3.33 eV, 3.35 eV, and 3.20 eV, respectively. SEM analysis showed that the nanoparticle shapes resembled flowers. Additionally, the assessment of antibacterial activity against pathogens, along with a comparative study, aids in evaluating the optimal utilization of nanoparticles in industries such as food packaging and cosmetics.

Keywords: *Colocasia esculenta; Murraya koenigii; Phyllanthus emblica; Psidium guajava;* Zinc Oxide.

[a] Department of Physics, Career Point University, Hamirpur, Himachal Pradesh-176041, India.
Centre for Nano-Science and Technology, Career Point University, Hamirpur, Himachal Pradesh-176041, India.

[b] Department of Biotechnology, School of Life Sciences, Central University of Rajasthan, Ajmer, Rajasthan-305801, India.

[c] Department of Biotechnology, School of Life Sciences, Central University of Rajasthan, Ajmer, Rajasthan-305801, India.

[d] Department of Animal Sciences, Central University of Himachal Pradesh, Kangra, Shahpur, Himachal Pradesh 176206, India.

[e] Department of Chemistry, Career Point University, Hamirpur, Himachal Pradesh-176041, India.
Centre for Nano-Science and Technology, Career Point University, Hamirpur, Himachal Pradesh-176041, India

[f] Department of Pharmaceutical Sciences, Career Point University, Hamirpur, Himachal Pradesh-176041, India.

[g] Department of Physics, Career Point University, Hamirpur, Himachal Pradesh-176041, India.
Centre for Nano-Science and Technology, Career Point University, Hamirpur, Himachal Pradesh-176041, India.
Corresponding author:
naveenthakur2327@gmail.com

INTRODUCTION

The development of nanoparticles from various metal salts has significantly advanced the field of health and medicine. The small size of nanoparticles has revolutionized nanotechnology due to their unique properties (Prakasham *et al.*, 2014). In the current era, scientists are keen to use environmentally friendly methods for nanoparticle production, primarily because of their cost-effectiveness and their potential as effective capping and stabilizing agents. This approach reduces reliance on chemicals and minimizes their adverse impacts. Living organisms play a crucial role in the biofabrication of metal oxide nanoparticles. Among all biological sources, plants are considered the best candidates for large-scale biosynthesis of nanoparticles

due to the diversity in size and shape of nanoparticles synthesized from them compared to those from other sources (Kumar *et al.*, 2024a). Green synthesis does not require the addition of surfactants or capping agents, as plant metabolites act as stabilizing agents (Rouhi *et al.*, 2013), which is a major advantage over chemical synthesis. Additionally, green synthesis is eco-friendly, simpler, and less costly than chemical methods. Plant extracts are non-toxic and use water as a medium for the preparation of biosynthesized nanoparticles (Kumar *et al.*, 2024b). Recently, researchers across various fields have shown interest in zinc oxide nanoparticles due to their distinctive properties and diverse applications (Baker *et al.*, 2013). Zinc oxide nanoparticles are utilized in both industrial and scientific areas (Kumar *et al.*, 2024c) because of their high excitonic binding energy and wide band gap at the nanoscale. Moreover, the biosynthesis of zinc oxide has a wide range of applications in the biological field, including antibacterial, antifungal, drug delivery, gene delivery, biological sensing, and anti-diabetic activities (Kolodziejczak *et al.*, 2014). In the past decade, numerous studies have reported the biosynthesis of zinc oxide using various plant extracts. Literature reveals that zinc oxide nanoparticles have been synthesized from leaf extracts of *Ocimumbasilicum L. var. purpurascens*, *Partheniumhysterophorus L.* (Kolodziejczak *et al.*, 2014), *Calotropisprocera*, *Aloe vera* (Singhai *et al.*, 1997), *Plectranthusamboinicus* (Kumar *et al.*, 2024d), *Citrus aurantifolia* (Thakur & Thakur, 2024a), *Artocarpusheterophyllus* (Rana *et al.*, 2024), *Laurusnobilis* (Samat *et al.*, 2013), *Annonasquamosa* (Thakur & Thakur, 2024b), and flower extracts of *Anchusaitalica* (Vijayakuma *et al.*, 2016), *Trifoliumpratense* (Thakur *et al.*, 2023), *Punicagranatum* (Azizi *et al.*, 2016); seed extracts of *Pongamiapinnata* (Dobrucka & Dlugaszewska, 2016) and *Cuminumcyminum* (Thakur *et al.*, 2024c); fruit extracts of *Borassusflabellifer* (Malaikozhundan *et al.*, 2017), *Emblicaofficinalis* (Zare *et al.*, 2017), and *Artocarpusgomezianus* (Thakur *et al.*, 2024d); root extracts of *Withaniasomnifera* (Anbukkarasi *et al.*, 2015) and *Rubusfairholmianus* (Anitha *et al.*, 2018); and peel extracts of *Musa sapientum* (Prasad *et al.*, 2021) and Punicagranatum (Rajendran *et al.*, 2021).

This investigation utilized leaf extracts from four distinct plants to synthesize zinc oxide nanoparticles: *Psidium guajava*, *Colocasia esculenta*, *Phyllanthus emblica*, and *Murraya koenigii Psidium guajava*, known for its medicinal properties, is associated with various biological activities, including antibacterial, antitussive, and antidiabetic effects (Ruangtong *et al.*, 2021). The other plants also demonstrated antibacterial and antimicrobial activities using different synthesis approaches. Zinc oxide (ZnO) nanoparticles are prized for their diverse applications. Using plant extracts for their synthesis offers a greener, eco-friendly alternative to traditional methods. Plant-based synthesis utilizes natural phytochemicals for reduction and stabilization, enhancing the nanoparticles' stability and biocompatibility while reducing environmental impact. Zinc oxide nanoparticles were synthesized using microwave techniques with these plant extracts, and the prepared nanoparticles were characterized using XRD, SEM, EDS, TEM, FTIR, and UV-spectroscopy to understand their morphology.

MATERIAL AND METHODOLOGY

Chemicals

To conduct the microwave-assisted synthesis of ZnO nanoparticles and evaluate their antibacterial activity, analytical research-grade Zinc acetate dihydrate ($(CH3COOH)_2Zn{\cdot}2H_2O$), Sodium hydroxide (NaOH), and Agar-agar Type I, Mueller Hinton broth, Nutrient agar was procured from Sigma. *Escherichia coli* (MTCC 739), *Staphylococcus aureus* (MTCC 737), and *Bacillus subtilis* (MTCC 441) were acquired from CSIR-IMTECH, Chandigarh.

Preparation of Plant Extracts

Fresh leaves of *Psidium guajava*, *Colocasia esculenta*, *Phyllanthus emblica* and *Murraya koenigii* plants were collected from the local area of Hamirpur, Himachal Pradesh. The leaves underwent meticulous chopping and were subsequently washed with tap water, followed by a rinse with distilled water, and finally air-dried. A quantity of 10 g of the dried leaves was then crushed and introduced into 100 ml of distilled water. The plant extract was formulated by boiling the mixture at 80 °C for 1 hour in a Soxhlet apparatus, which was sterilized with ethanol before preparing the plant extract. After cooling, the resultant solutions were filtered with Whatman filter paper to acquire a transparent plant extract solution. These plant extracts were stored in a refrigerator at 4 °C for subsequent experimentation.

 https://doi.org/10.37819/nanofab.9.2035

EXPERIMENTAL PROCEDURE

For the preparation of zinc oxide nanoparticles, 100 ml of 0.005M zinc acetate dihydrate salt solution was prepared by continuous stirring for 60 minutes on a magnetic stirrer. To synthesize nanoparticles mediated by *Psidium guajava*, 10 ml of the plant extract was carefully added drop by drop into the salt solution and stirred for 60 minutes. Subsequently, a 2 M NaOH solution was introduced gradually into the mixture to attain a pH level of 12. Thereafter, the solution was placed inside a preheated domestic microwave at 200 °C for 10 min. The resulting precipitates were thencooled and filtered into another vessel for washing. The resulting precipitate underwent 2-3 washes with both distilled water and ethanol. Subsequently, the precipitate was subjected to drying in an oven at 70 °C for 8 hours to yield ZnO nanoparticles. A schematic diagram depicting the green synthesis of ZnO nanoparticles is presented in Fig. 1. The identical procedure was employed for the synthesis of Zinc oxide nanoparticles mediated by plant extracts from *Colocasia esculenta*, *Phyllanthus emblica*, and *Murraya koenigii*.

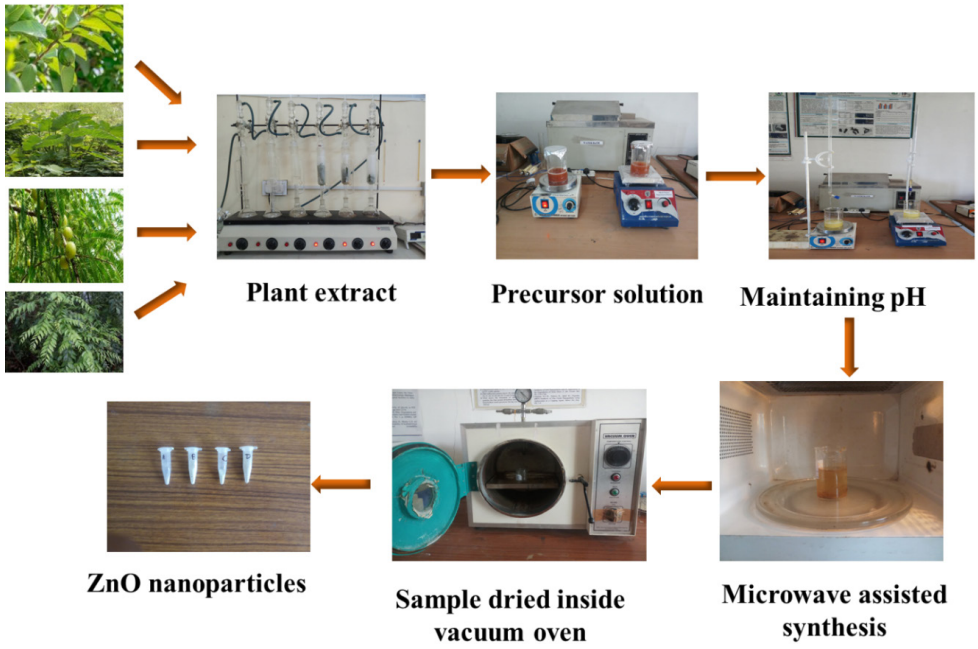

Figure 1. Schematic representation of green synthesis of ZnO nanoparticles using microwave technique.

CHARACTERIZATION

The structural features of ZnO nanoparticles formed with different plant extracts were obtained by using an X-ray diffractometer, TEM/SEM, EDS, FTIR, and UV-vis spectrophotometer. The XRD analysis usually provides information regarding the crystalline nature, lattice formation, and crystalline grain size of matter. A radiation source of CuKα was used to produce X-rays of wavelength, $\lambda = 0.154$ nm. A Quanta 2000 microscope was used to record SEM micrographs. Further, EDS (energy dispersive X-ray) has been used to recognize the composition of resultant nanoparticles. TEM, FTIR and UV- spectroscopy have also been performed to understand the morphology, and to identify the compounds and optical properties of synthesized samples. The initial characterization of ZnO nanoparticles of *Psidium guajava*, *Colocasia esculenta*, *Phyllanthus emblica* and *Murraya koenigii* was performed using a UV-vis spectrophotometer. The technique was used to calculate the bandgap of synthesized nanoparticles at a wavelength range of 200-800 nm present in a suspension. Bandgap and spacing of the electronic level are in an inversely proportional relationship with the size of nanoparticles, the more the bandgap the lesser the size of particles. Such phenomenon is commonly termed as "quantum size effect". The bandgap energy (E) of the synthesized zinc oxide nanoparticles was calculated utilizing Planck's equation, as expressed in equation (1).

$$Eg = \frac{hc}{\lambda} = \frac{1240}{\lambda} \quad (1)$$

Here, Eg represents the energy bandgap in electron volts (eV), h stands for the Planck constant with a value of 6.626×10^{-34} J/s, c denotes the speed of light equal to 3×10^8 m/s, and λ_{max} signifies the maximum absorption wavelength measured in nanometers (nm).

ANTIBACTERIAL ACTIVITY OF ZnO NANOPARTICLES

The agar well diffusion method was employed to evaluate the antimicrobial characteristics of ZnO nanoparticles synthesized through green methods. Three different concentrations of each of the four nanoparticle types were examined to assess their efficacy as antibacterial agents against one Gram-negative bacterium *(Escherichia coli)* and two Gram-positive bacteria *(Bacillus subtilis* and *Staphylococcus aureus)* (Sukri *et al.*, 2019).To culture bacteria, first prepare and sterilize a growth medium, such as nutrient agar or broth, through autoclaving. Inoculate the medium with the bacterial sample using a sterile loop or pipette. Incubate the inoculated medium at 35-37°C for 18-24 hours, or as required for the specific bacterial strain. After incubation, evaluate bacterial growth by inspecting for colonies on agar plates or turbidity in liquid cultures. For isolation and further study, streak colonies onto fresh agar plates to obtain pure cultures. Store cultures long-term via freezing and short-term in a refrigerator.

RESULT AND DISCUSSION

XRD Analysis

XRD was performed to confirm the existence of ZnO nanoparticles along with their structural parameters. The XRD patterns corresponding to Zinc oxide nanopowders synthesized with four different plant extracts by microwave technique are displayed in Fig. 2. The information provided in x-ray peaks helps to obtain crystallite aspects. Similar patterns are exhibited in all four samples. Reflected planes (100), (002), (101), (102), (110), (103), (112) and (201) correspond to Bragg angle's 31.9°, 34.5°, 36.3°, 47.6°, 56.7°, 62.9°, 68.1° and 69.1° are indicating toward ZnO hexagonal structure. These results are compared with JCPDS 36-1541 (Rehan *et al.*, 2019) that were reported in previous literature. Maximum intensity of the (101) plane in all four samples assures the materialization of the hexagonal wurtzite structure.

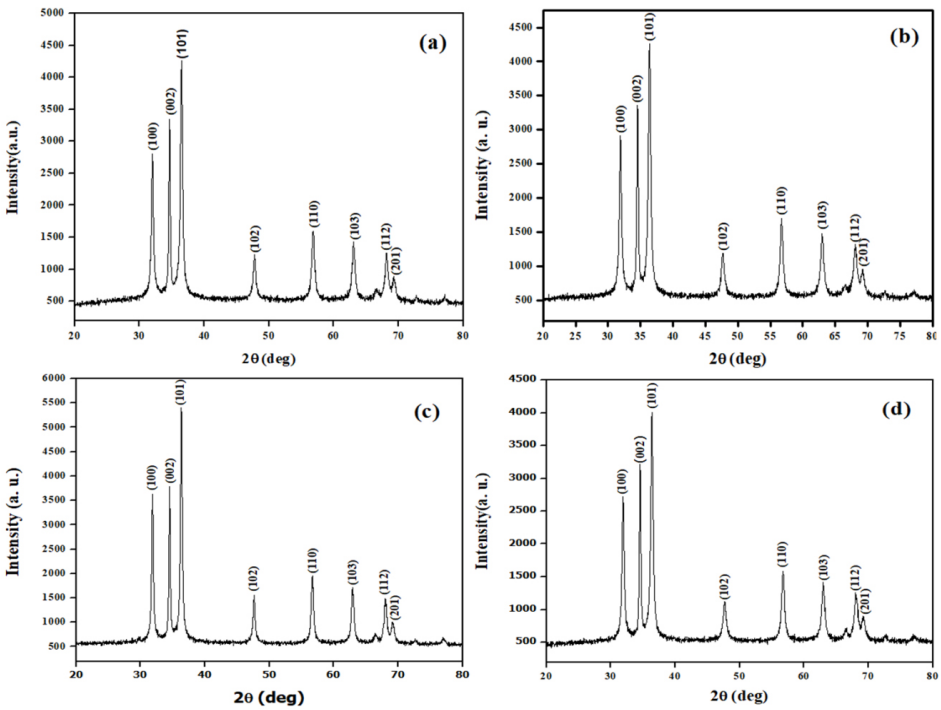

Figure 2. XRD peaks specifying the existence of ZnO. (a) *Psidium guajava*, (b) *Colocasia esculenta*, (c) *Phyllanthus emblica* and (d) *Murraya koenigii*, leaves directed ZnO nanoparticles.

 https://doi.org/10.37819/nanofab.9.2035

The ZnO structural parameters such as lattice parameters (a = b, c), degree of crystallinity (χ^c) (Sharma *et al.*, 2021), crystallite size (D) (Sun *et al.*, 2011), microstrain (ε) (Ren *et al.*, 2009), stacking fault (α) (and Dislocation density (δ) [33] are calculated by using empirical relations are mentioned as follow:

$a = b = (\lambda/(3^{1/2}\sin\theta)$

$c = (\lambda/\sin\theta)$

$\chi^c = (0.24/\beta)^3$

$D = 0.9\ \lambda/\beta\cos\theta$

$\varepsilon = \beta/4\tan\theta$

$\alpha = \frac{2\pi^2}{45(3\tan\theta)^{1/2}}\beta$

$\delta = 1/(D)^2$

Whereas λ, θ and β represent x-ray wavelength, Bragg's angle and FWHM (Full width at half maxima). Table 1 provides calculated structural parameters by using XRD data and above mention empirical relations.

S. No.	Structural parameters	Samples	2θ (deg)	FWHM (β)	Formula Used	Results
1	a*(Å)*	(a) (b) (c) (d)	31.09	0.31 0.32 0.28 0.32	$(\lambda/(3^{1/2}\sin\theta)$	3.20 nm
2	c*(Å)*	(a) (b) (c) (d)	34.5	0.31 0.32 0.28 0.32	$(\lambda/\sin\theta)$	5.12 nm
3	χ^c	(a) (b) (c) (d)	34.5	0.31 0.32 0.28 0.32	$(0.24/\beta)^3$	0.464 0.421 0.629 0.421
4	D(nm)	(a) (b) (c) (d)	36.3	0.45 0.5 0.37 0.49	$0.9\ \lambda/\beta\cos\theta$	14.22 nm 12.80 nm 17.30 nm 13.06 nm
5	ε	(a) (b) (c) (d)	36.3	0.45 0.5 0.37 0.49	$\beta/4\tan\theta$	6.44×10^{-4} 7.15×10^{-4} 5.29×10^{-4} 7.01×10^{-4}
6	α	(a) (b) (c) (d)	36.3	0.45 0.5 0.37 0.49	$\frac{2\pi^2}{45(3\tan\theta)^{1/2}}\beta$	0.199206 0.22134 0.163792 0.216914

Table 1. Calculated results for structural parameters by using XRD data.

S. No.	Samples	2θ (deg)	FWHM (β)	D (nm)	Formula Used	Δ
01	(a)	36.3	0.45	14.22 nm	$1/(D)^2$	4.94×10^{-3}
02	(b)		0.5	12.80 nm		6.10×10^{-3}
03	(c)		0.37	17.30 nm		3.34×10^{-3}
04	(d)		0.49	13.06 nm		5.86×10^{-3}

Table 2. Calculated results for Dislocation density for samples by using XRD data.

Dislocation density (δ) has alsobeencalculated which is mentioned in Table 2. Strain represents imperfection or defect in a crystal with the arrangement of lattice constants (Karthik *et al.*, 2020). Bond length changes due to the variation in lattice constant that results in strain and charge carrier gradient responsible for the shrinkage of the crystallite in the crystal structure (Mobarak *et al.*, 2022).The lower value of strain in sample (c) suggests that zinc oxide nanoparticles synthesized with *Phyllanthus emblica* have more crystallinity as compared to other samples which can also be seen in the values of degree of crystallinity.

SEM and EDAX Analysis

Scanning Electron Microscopy is performed to understand the morphology of synthesized Zinc oxide with different plant extracts. (Fig. 3) shows SEM results for all synthesized samples. Fig. 3 (a-d) indicates that pure Zinc oxide samples prepared by microwave technique have flower flake shapes and are abundantly distributed regularly. The average flower size was calculated as 637 nm for sample A, 282 nm for sample B, 813 nm for sample C and 735 nm for sample D by using ImageJ software from SEM results. The variation in average sizes of samples is due to the usage of different plant extracts. Also, there is no contact of nanoparticles with each other in samples, which indicates the stability of particles by reducing agent (Bindu *et al.*, 2014).

The Energy-dispersive X-ray analysis has also been performed for all synthesized samples as shown in (Fig. 4). This analysis is done to know the atomic as well as weight percentage of elements present in samples. (Fig. 4) confirms the presence of pure Zinc oxide of Zn and O elements without any impurity, whoseatomic and weight percentages are also given in tabular format.

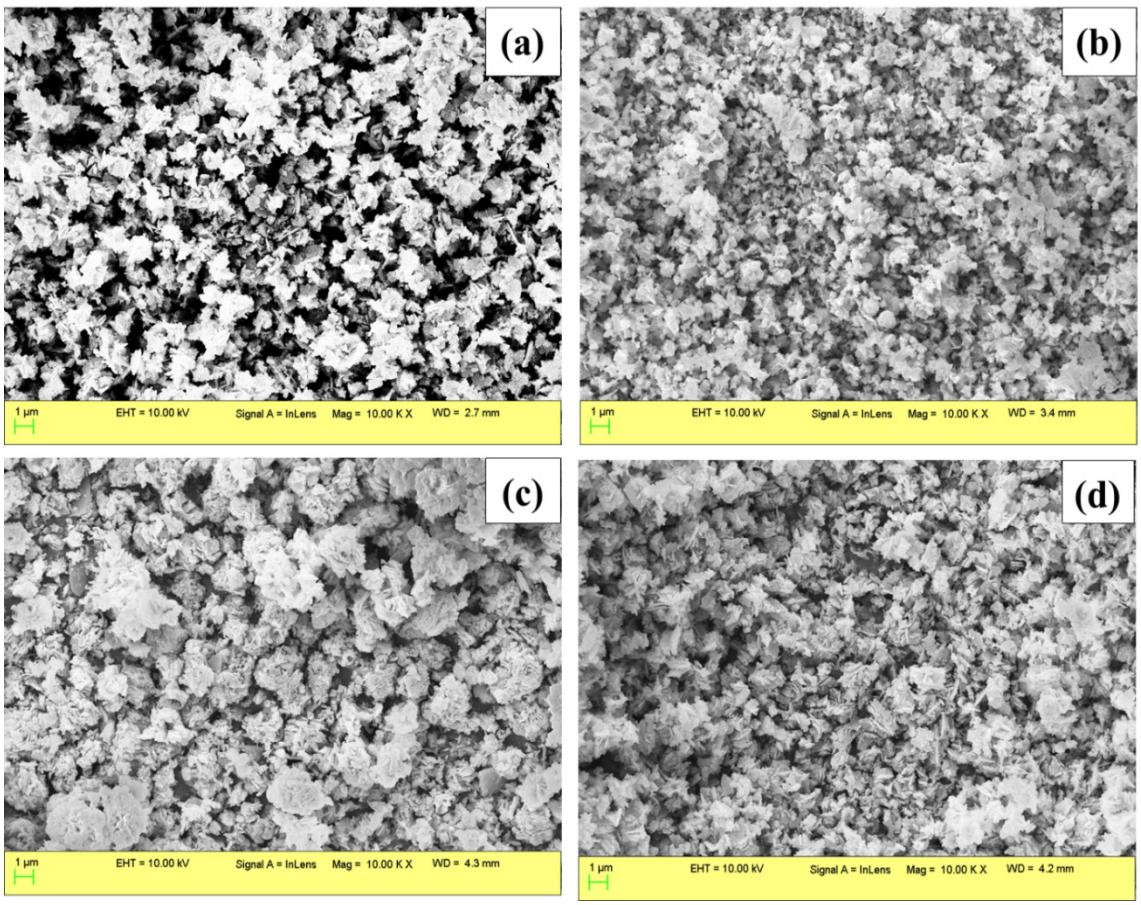

Figure 3. SEM images for synthesized ZnO nanoparticles with (a) *Psidium guajava*, (b) *Colocasia esculenta*, (c) *Phyllanthus emblica* and (d) *Murraya koenigii.*

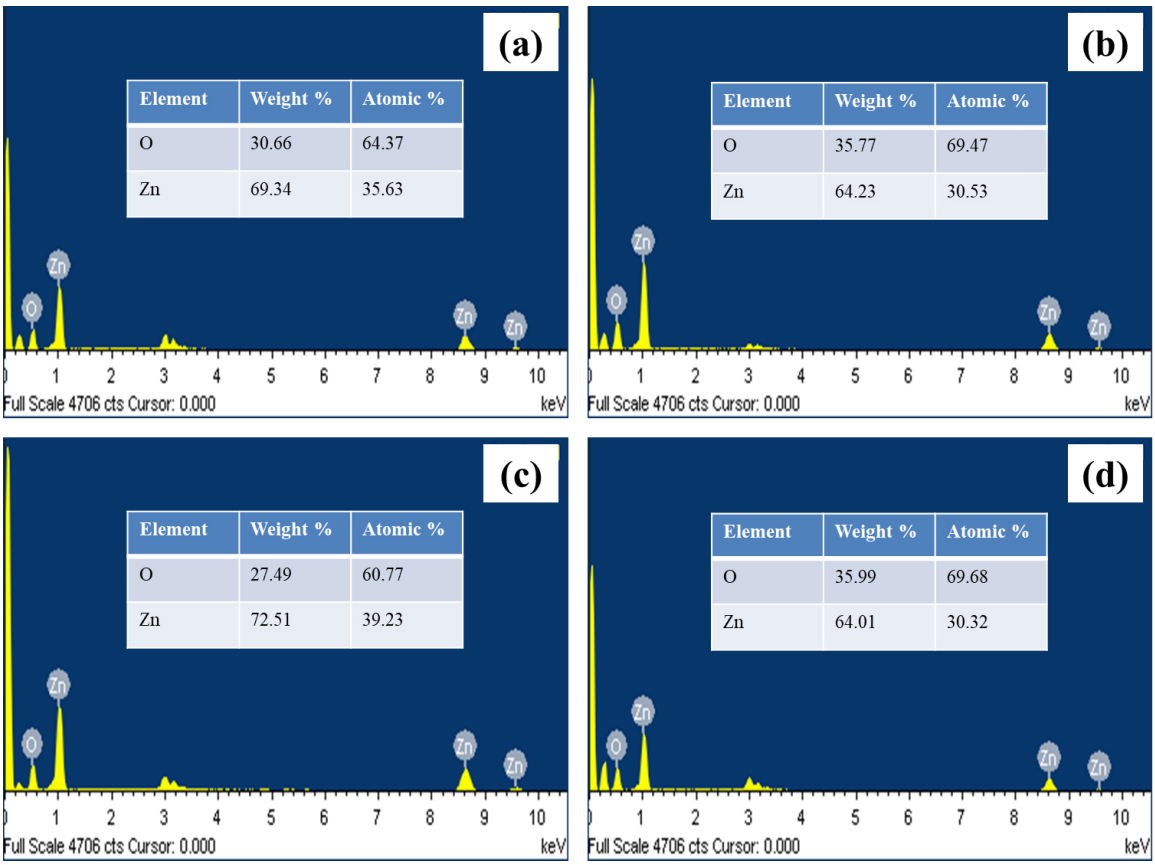

Figure 4. EDAX graphs with elemental composition for samples. (a) *Psidium guajava,* (b) *Colocasia esculenta*, (c) *Phyllanthus emblica* and (d) *Murraya.*

TEM

TEM images in Fig. 5 (a-d) of synthesized ZnO nanoparticles with *Psidium guajava*, *Colocasia esculenta*, *Phyllanthus emblica*, and *Murraya koenigii* reveal that the nanoparticles exhibit irregular shapes, including spherical ones. Displayed histograms in Fig. 5 (a-d) help to determine the average size of nanoparticles as shown in Table 3. The average particle sizes for samples (a), (b), (c), and (d) were 19 nm, 15.12 nm, 16.09 nm, and 23.81 nm, respectively, as determined using ImageJ software. Variations in particle size were observed due to the use of different plant extracts.

S. No.	Sample (a), (b), (c) & (d)	Size of nanoparticles (range)	Maximum distribution of nanoparticles (range)	Average size (nm)
01	ZnO - *Psidium guajava*	05 – 45 nm	15 – 25 nm	19 nm
02	ZnO - *Colocasia esculenta*	05 – 30 nm	05 – 10 nm	15.12 nm
03	ZnO - *Phyllanthus emblica*	05 – 35 nm	10 – 20 nm	16.09 nm
04	ZnO - *Murraya koenigii*	10 – 90 nm	10 – 30 nm	23.81 nm

Table 3. Exploration of histograms displayed in Fig. 3 (a-d).

Moreover, SAED (Selected Area Electron Diffraction) patterns for all synthesized samples are displayed in Fig. 5 (a-d). ImageJsoftware is used to calculate the estimated inter-planner distance or d-spacing as displayed in supplementary information as Table 4, where r represents the radius of concentric circles that have been plotted in the SAED pattern.

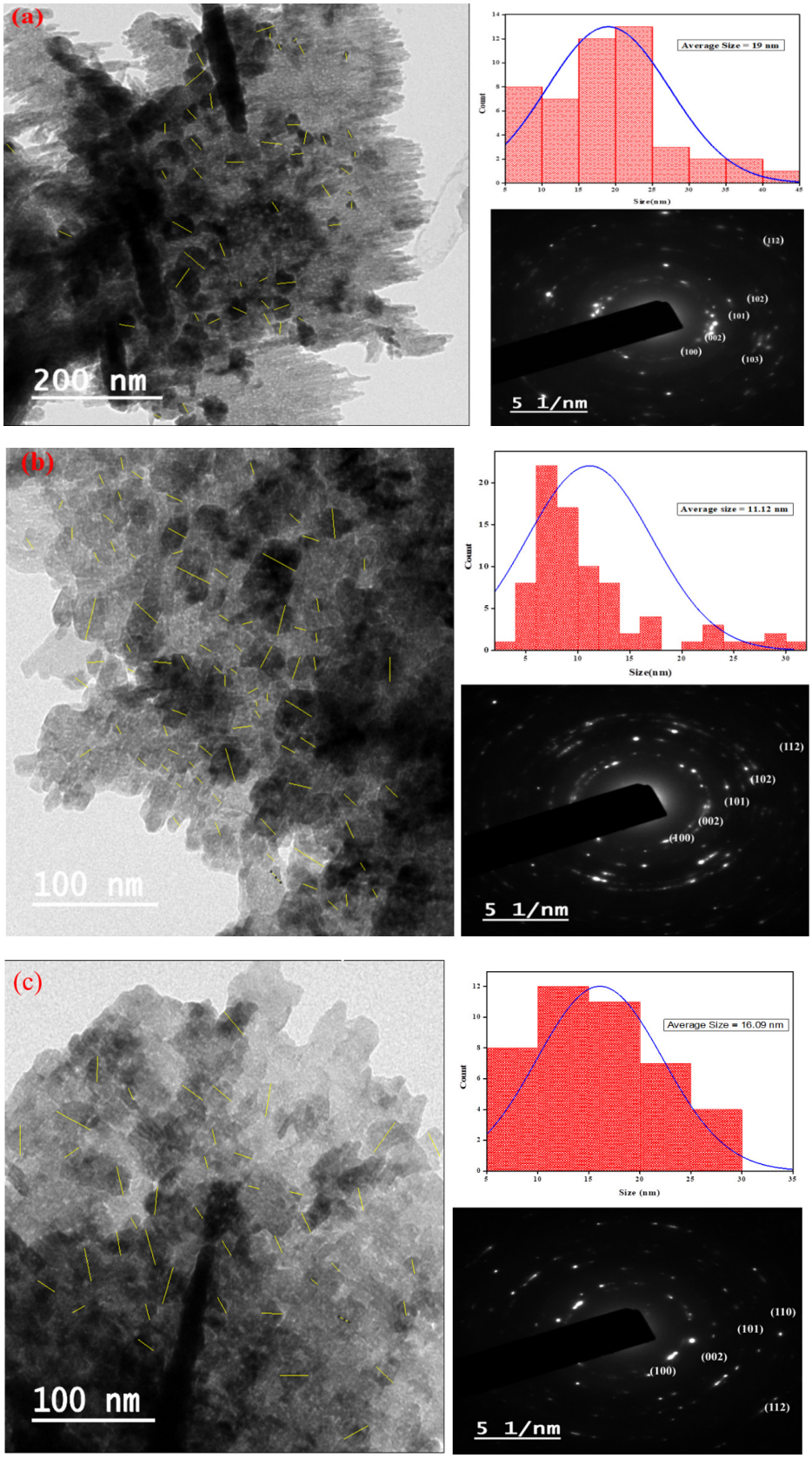

 https://doi.org/10.37819/nanofab.9.2035

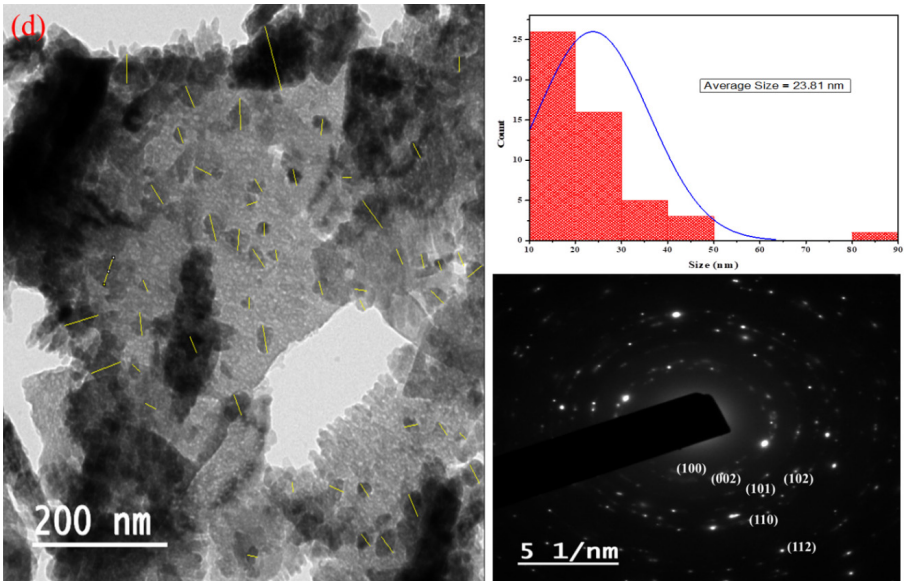

Figure 5. TEM and SAED images for samples. (a) *Psidium guajava*, (b) *Colocasia esculenta*, (c) *Phyllanthus emblica* and (d) *Murraya koenigii*.

Hexagonal wurtziteZnO (JCPDS No. 00-036-1451)		Sample (a)			Sample (b)		
(hkl)	d(A°)	1/2r	r (nm)	d-spacing	1/2r	r (nm)	d-spacing
100	2.81430	7.121	0.280859	2.808594	7.101	0.28165	2.816505
002	2.60332	7.688	0.260146	2.601457	7.683	0.260315	2.60315
101	2.47592	8.051	0.248416	2.484163	8.051	0.248416	2.484163
102	1.91114	10.448	0.191424	1.914242	10.508	0.190331	1.903312
103	1.47712	13.726	0.145709	1.457089	—	—	—
112	1.37818	14.559	0.137372	1.373721	14.559	0.137372	1.373721
Hexagonal wurtziteZnO (JCPDS No. 00-036-1451)		**Sample (c)**			**Sample (d)**		
(hkl)	d(A°)	1/2r	r (nm)	d-spacing	1/2r	r (nm)	d-spacing
100	2.81430	6.998	0.285796	2.857959	7.078	0.282566	2.825657
002	2.60332	7.678	0.260485	2.604845	7.708	0.259471	2.594707
101	2.47592	8.151	0.245369	2.453687	8.051	0.248416	2.484163
102	1.91114	—	—	—	10.521	0.190096	1.90096
110	1.62472	12.208	0.163827	1.63827	12.298	0.162628	1.626281
112	1.37818	14.609	0.136902	1.369019	14.592	0.137061	1.370614

Table 4. Comparison of calculated d-spacing of all samples with reported results

FTIR Analysis

The synthesized zinc oxide nanoparticles have been examined in the range of 4000-600 cm^{-1} to ensure the appearance of functional groups through the FTIR spectrum, as shown in Fig. 6. It has been observed that strong broad peaks of O-H stretching lie between 3550 and 3200 cm^{-1} in all samples (Koutu *et al.*, 2016). Furthermore, in all synthesized samples, a robust stretching of O=C=O appeared at 2359 cm^{-1} for sample (a), 2351 cm^{-1} for sample (b), 2352 cm^{-1} for sample (c), and 2359 cm^{-1} for sample (d), respectively, attributable to the presence of CO_2 in the air. Peaks at 1571 cm^{-1} in sample (b) and 1578 cm^{-1} in sample (d) corresponded to C=C stretching (cyclic alkene). Within the range of 1420 to 1330 cm^{-1}, peaks indicative of O-H bending (alcohol) were observed in all samples. The broader and weaker bands, located near 900 cm^{-1} in sample (a), 902 cm^{-1} in sample (b), 867 cm^{-1} in sample (c), and 874 cm^{-1} in sample (d),

represented N-H bending vibrations of amines [Song *et al.*, 2008; Farzana *et al.*, 2015). The results show a range of peak absorptions below 850 cm^{-1}. Specifically, the peak near 664 cm^{-1} is commonly linked to bending vibrations of hydroxyl (O-H) groups or possibly to bending vibrations of C-H bonds in alkanes (MaslowskyJr, 2019). Likewise, the peak at 671 cm^{-1} may also correspond to bending vibrations of O-H or C-H bonds (Kloprogge *et al.*, 2004). These peaks might reflect specific interactions or bonding within the sample, such as metal-oxygen bonds in metal oxides or other complex structures.

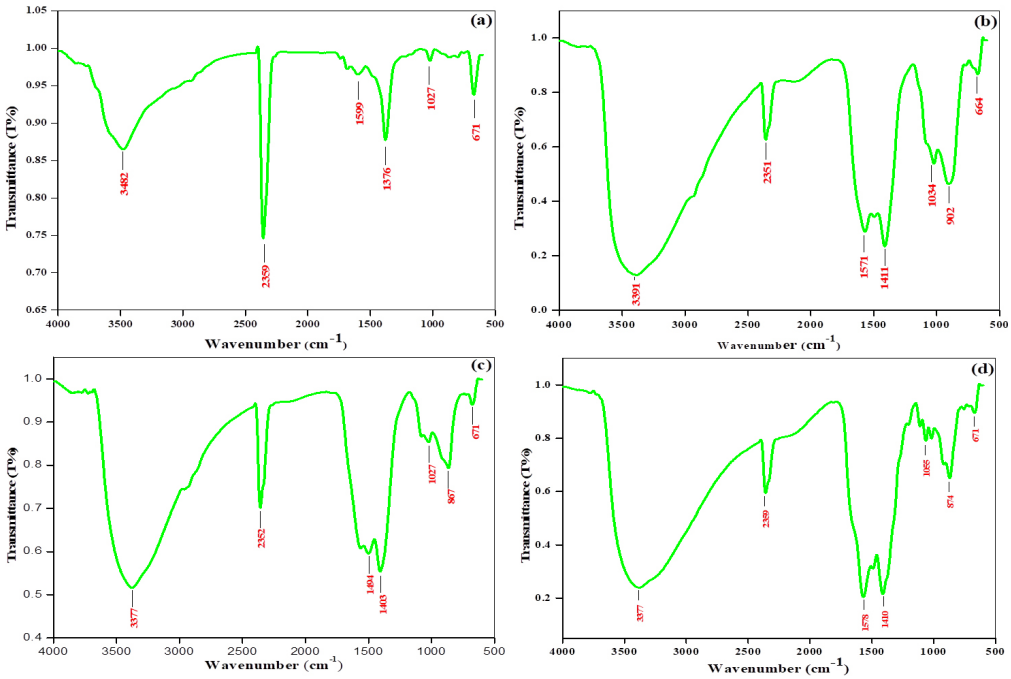

Figure 6. FTIR graphs for samples. (a) *Psidium guajava,* (b) *Colocasia esculenta,* (c) *Phyllanthus emblica* and (d) *Murraya koenigii.*

UV-Vis Spectroscopy

The bandgap values for the synthesized zinc oxide nanoparticles were determined as 3.28, 3.33, 3.35, and 3.20eV for *Psidium guajava*, *Colocasia esculenta*, *Phyllanthus emblica*, and *Murraya koenigii*, respectively, as depicted in Fig. 7. Sample's forbidden energy gap determined using the Tauc plot (Verma *et al.*, 2024). Absorbance is subject to modification based on various factors, including particle size and the presence of oxygen deficiencies within the synthesized material (Pai *et al.*, 2019) as shown in Fig. 8.

Absorbance is subject to modification based on various factors, including particle size and the presence of oxygen deficiencies within the synthesized material (Pai *et al.*, 2019) as shown in Fig. 8. Changes in the valence band edge toward the lower side and the conduction band edge toward the upper side can occur, leading to interactions between s-d and p-d exchange, resulting in an increased bandgap (Mirza *et al.*, 2019). These structural modifications can alter the mass density, resulting in diverse electronic configurations. UV absorbance spectra indicate that the synthesized zinc oxide nanoparticles function as catalysts under UV light, generating OH radicals with the potential to create a charge for bacterial elimination during antibacterial activity (Dadi *et al.*, 2019).

Antibacterial Activity

The good diffusion method was employed to investigate the antibacterial activity of the synthesized nanoparticles against Gram-positive bacteria *(Bacillus subtilis* and *Staphylococcus aureus)* and Gram-negative bacteria *(Escherichia coli)* (Saha *et al.*, 2018). To assess antibacterial activity using the good diffusion method, begin by preparing a Mueller-Hinton agar plate and allowing it to solidify. Inoculate the surface of the agar with a standardized bacterial suspension to create an even bacterial

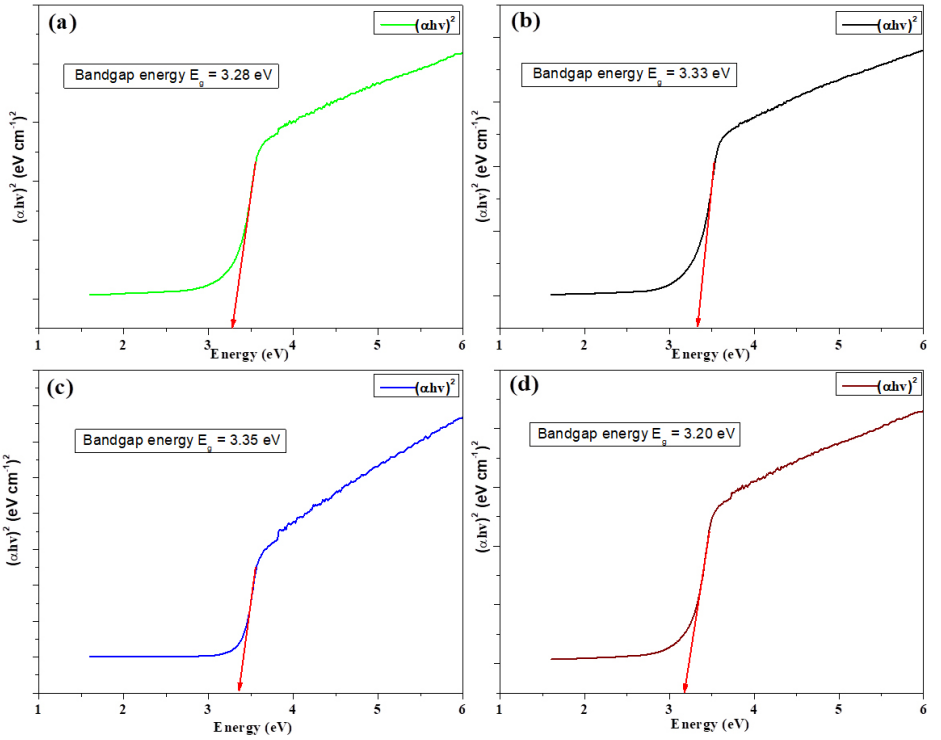

Figure 7. Band gap for samples (a) *Psidium guajava*, (b) *Colocasia esculenta*, (c) *Phyllanthus emblica* and (d) *Murraya koenigii*.

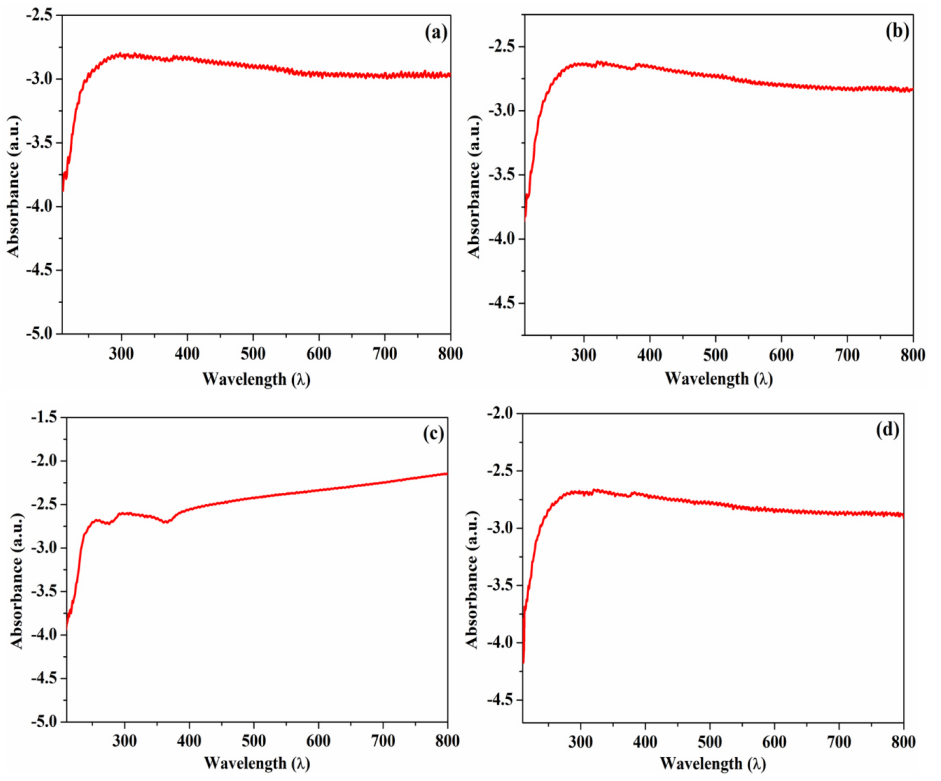

Figure 8. UV spectra for samples (a) *Psidium guajava*, (b) *Colocasia esculenta*, (c) *Phyllanthus emblica* and (d) *Murraya koenigii*.

lawn. Once the plate is inoculated, use a sterile cork borer or similar tool to create wells in the agar. Add the synthesized NPs, in specific ratios, into these wells. Incubate the plate at 35-37°C for 18-24 hours to promote bacterial growth. After incubation, observe and measure the clear zones of inhibition around each well. These zones indicate the effectiveness of the test substance, with larger zones reflecting greater antibacterial activity. (Fig. 9) clearly illustrates the observed zone of inhibition for all synthesized samples at varying low concentrations (5, 15, and 25 mg/ml).

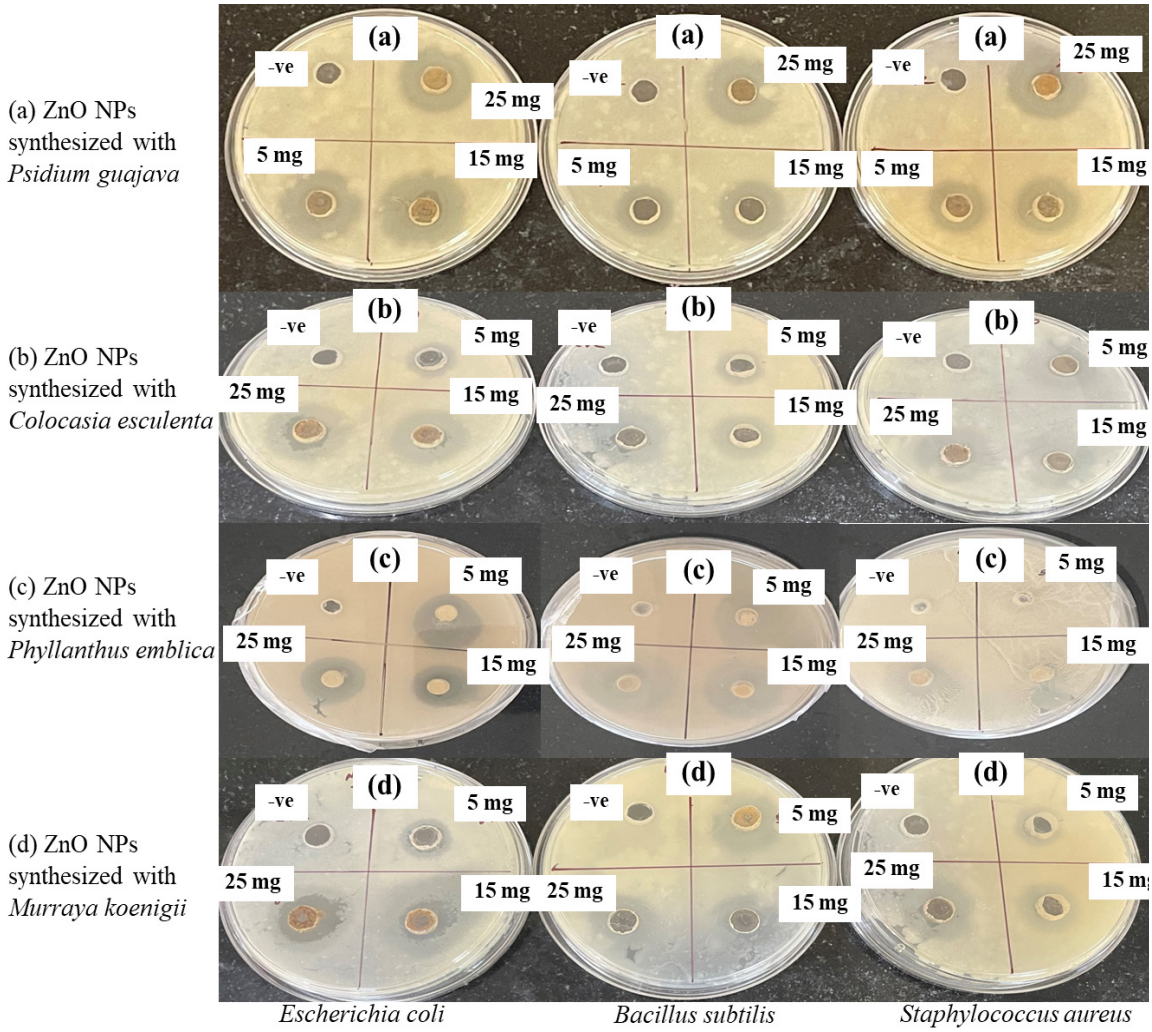

Figure 9. The Zone of inhibition of nanoparticles corresponds to different bacterial strains. (a) *Psidium guajava,* (b) *Colocasia esculenta,* (c) *Phyllanthus emblica* and (d) *Murraya koenigii.*

Sample (a) exhibited the highest and most consistent antibacterial effectiveness, with significant zones of inhibition observed across all concentrations, showing a peak activity at 25 mg/ml. In contrast, sample (b) displayed greater variability; although inhibition increased with concentration, the activity at lower concentrations was notably less effective. Sample (c) showed moderate activity, with increasing inhibition at higher concentrations but generally lower effectiveness compared to sample (a). Sample (d) had the least overall antibacterial activity, with lower zones of inhibition at all tested concentrations. These findings indicate that the synthesis conditions and concentration of ZnO NPs greatly influence their antibacterial efficacy, with sample (a) & (b) providing the most pronounced and consistent results as shown in Table 5. Higher efficiency for antibacterial activity is also seen in previous literature (Saha et al., 2018; Ramya *et al.*, 2022).

 https://doi.org/10.37819/nanofab.9.2035

Synthesized ZnO NPs samples	Bacteria	Nanoparticle concentration (mg/ml)	ZOI (Zone of Inhibition) (mm)
(a)	*Escherichia coli*	5	18
		15	17
		25	18
	Bacillus subtilis	5	14
		15	18
		25	24
	Staphylococcus aureus	5	15
		15	19
		25	24
(b)	*Escherichia coli*	5	08
		15	16
		25	24
	Bacillus subtilis	5	08
		15	15
		25	22
	Staphylococcus aureus	5	09
		15	17
		25	23
(c)	*Escherichia coli*	5	10
		15	18
		25	24
	Bacillus subtilis	5	10
		15	17
		25	23
	Staphylococcus aureus	5	06
		15	08
		25	10
(d)	*Escherichia coli*	5	08
		15	16
		25	20
	Bacillus subtilis	5	10
		15	14
		25	16
	Staphylococcus aureus	5	06
		15	10
		25	18

Table 5. Comparison of ZOI of all samples at different concentrations against Gram-positive and Gram-negative bacteria

The mechanisms of production of oxidative species due to the introduction of metal oxides inside the bacterial cells and the damage to the bacterial cell wall can be found in previous literature (Qidwai *et al.*, 2018). However, there are three possible steps in the antibacterial activity mechanism: (i) formation of ROS (reactive oxygen species), (ii) damage of the cell wall, and (iii) ion reduction (Siddiqi *et al.*, 2018; Elumalai *et al.*, 2015). Mechanism of antibacterial activity of synthesized nanoparticles as shown in Fig. 10. ZnO nanoparticles exhibit antibacterial activity through several mechanisms: they generate reactive oxygen species (ROS) that damage bacterial cells, directly disrupt cell membranes, release Zn^{2+} ions that interfere with bacterial processes, and exhibit photocatalytic activity

under UV light to produce additional ROS. Their high surface area also enhances their reactivity and interaction with bacterial cells, contributing to their overall antimicrobial effectiveness. Higher efficiency and smaller nanoparticle sizes can exhibit higher antibacterial activity. The antibacterial results have been compared with previous studies involving *Escherichia coli* and *Staphylococcus aureus* pathogens tested against ZnO nanoparticles synthesized through green and chemical methods, as detailed in Table 6. From this analysis, we conclude that our synthesized ZnO nanoparticles can be used as food packing material to inhibit bacterial growth and keep food hygienic for a long time.

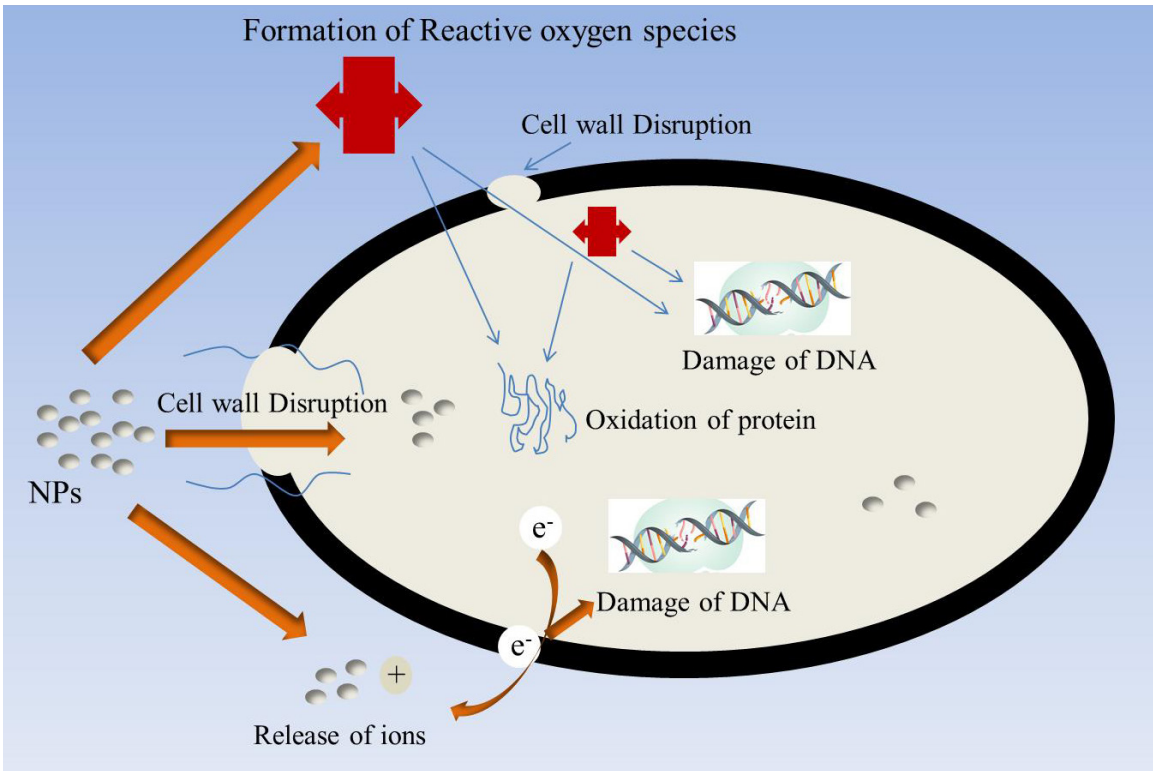

Figure 10. Mechanism for Antibacterial activity of synthesized nanoparticles

S. No.	Pathogens	Synthesized method	Plant extract	Crystallite size (nm)	Concentration of ZnO NPs	ZOI (mm)	References
01	*Staphylococcus aureus*	Chemical method	*Tamarindu-sindica*	19-37 nm	200 mg/l	13.1 ± 0.28	(Rajabi *et al.*, 2017)
02	*Staphylococcus aureus*	Green method	*Suaeda aegyptiaca*	60 nm	10 mg/ml	16.01	(Mahendra *et al.*, 2017)
03	*Escherichia coli*	Green method	*Cochlos-permum religiosum*	7 nm	1 mg/disc	19.36	(Madan *et al.*, 2016)
04	*Staphylococcus aureus*	Green method	*Cochlos-permum religiosum*	7 nm	1 mg/disc	22.20	
05	*Bacillus subtilis*	Microwa-ve-assis-ted green approach	*Psidium guajva*	14.22 nm	25 mg/ml	30	Present work
	Staphylococcus aureus						
	Escherichia coli		*Murraya koenigii*	13.09 nm		16	

Table 6. Comparison of ZOI of present work with literature

 https://doi.org/10.37819/nanofab.9.2035

CONCLUSION

In this study, we have mentioned the microwave technique for the synthesis of flower-shaped ZnO nanoparticles using four different plant extracts. Plant extracts as stabilizers reduced the crystallite size of synthesized samples, and hence we have reported the size of samples in the range of 12-17 nm through XRD analysis. The flower flake shapes of samples were confirmed by SEM and TEM analysis further helped to understand the morphology of the samples. FTIR analysis confirms the presence of functional groups inside the nanoparticles, which help enhance the antibacterial strength of nanoparticles. Moreover, the band-gap of nanoparticles was calculated with the analysis of UV-vis spectroscopy and found to be 3.34, 3.52, 3.35, and 3.33, which correspond to *Psidium guajava*, *Colocasia esculenta*, *Phyllanthus emblica*, and *Murraya koenigiileaf* extracts. The present work can be utilized by the food packaging industry with effective results in antibacterial activity. Moreover, the efficiency of synthesized nanoparticles can be increased by adding dopants for multiple applications.

Ethical Approval

Not required.

Consent to Participate

Not required.

Consent to Publish

Not required.

Authors Contributions

Conception and design of the study: N. Verma, N. Thakur

Acquisition of data: N. Verma, N. Thakur

Analysis and/or interpretation of data: N. Verma, L. Loveleen, S. Nimesh, N. Thakur

Drafting the manuscript: N. Verma, L. Loveleen, K. Jeet, N. Thakur

Revising the manuscript critically for important intellectual content: S. Nimesh, N. Thakur

Approval of the version of the manuscript to be published: Nirdosh Verma, Lacy Loveleen, Surendra Nimesh, Kamal Jeet and Naveen Thakur

Funding

No funding

Conflict of Interest

The authors declare no competing financial interest

Availability Statement

Data will be made available on request. ♦

REFERENCES

Anbukkarasi, V., Srinivasan, R., & Elangovan, N. (2015). Antimicrobial activity of green synthesized zinc oxide nanoparticles from Emblicaofficinalis. Int. J. Pharm. *Sci. Rev. Res*, *33*(2), 110-115.

Anitha, R., Ramesh, K. V., Ravishankar, T. N., Kumar, K. S., & Ramakrishnappa, T. (2018). Cytotoxicity, antibacterial and antifungal activities of ZnO nanoparticles prepared by the Artocarpusgomezianus fruit mediated facile green combustion method. *Journal of Science: Advanced Materials and Devices*, *3*(4), 440-451. https://doi.org/10.1016/j.jsamd.2018.11.001

Azizi, S., Mohamad, R., Bahadoran, A., Bayat, S., Rahim, R. A., Ariff, A., & Saad, W. Z. (2016). Effect of annealing temperature on antimicrobial and structural properties of bio-synthesized zinc oxide nanoparticles using flower extract of Anchusaitalica. *Journal of Photochemistry and Photobiology B: Biology*, *161*, 441-449. https://doi.org/10.1016/j.jphotobiol.2016.06.007

Baker, S., Rakshith, D., Kavitha, K. S., Santosh, P., Kavitha, H. U., Rao, Y., & Satish, S. (2013). Plants: emerging as nanofactories towards facile route in synthesis of nanoparticles. *BioImpacts: BI*, *3*(3), 111. doi: 10.5681/bi.2013.012

Bindu, P., & Thomas, S. (2014). Estimation of lattice strain in ZnO nanoparticles: X-ray peak profile analysis. *Journal of Theoretical and Applied Physics*, *8*, 123-134. https://doi.org/10.1007/s40094-014-0141-9

Dadi, R., Azouani, R., Traore, M., Mielcarek, C., & Kanaev, A. (2019). Antibacterial activity of ZnO and CuO nanoparticles against gram positive and gram negative strains. *Materials Science and Engineering: C*, *104*, 109968. https://doi.org/10.1016/j.msec.2019.109968

Dobrucka, R., & Długaszewska, J. (2016). Biosynthesis and antibacterial activity of ZnO nanoparticles using Trifoliumpratense flower extract. *Saudi Journal of Biological Sciences, 23*(4), 517-523. https://doi.org/10.1016/j.sjbs.2015.05.016

Elumalai, K., Velmurugan, S., Ravi, S., Kathiravan, V., & Ashokkumar, S. (2015). *RETRACTED: Facile, eco-friendly and template free photosynthesis of cauliflower like ZnO nanoparticles using leaf extract of Tamarindusindica (L.) and its biological evolution of antibacterial and antifungal activities.* https://doi.org/10.1016/j.saa.2014.09.129

Farzana, M. H., & Meenakshi, S. (2015). Visible light-driven photoactivity of zinc oxide impregnated chitosan beads for the detoxification of textile dyes. *Applied Catalysis A: General, 503*, 124-134. https://doi.org/10.1016/j.apcata.2014.12.034

Hossain, M. S., Mahmud, M., Mobarak, M. B., & Ahmed, S. (2022). Crystallographic analysis of biphasic hydroxyapatite synthesized by different methods: an appraisal between new and existing models. *Chemical Papers*, 1-13. https://doi.org/10.1007/s11696-021-01949-5

Karthik, K., Pushpa, S., Naik, M. M., & Vinuth, M. (2020). Influence of Sn and Mn on structural, optical and magnetic properties of spray pyrolysed-CdS thin films. *Materials Research Innovations*. https://doi.org/10.1080/14328917.2019.1597436

Koutu, V., Shastri, L., & Malik, M. M. (2016). Effect of NaOH concentration on optical properties of zinc oxide nanoparticles. *Materials Science-Poland, 34*(4), 819-827. DOI: 10.1515/msp-2016-0119

Kloprogge, J. T., Hickey, L., & Frost, R. L. (2004). FT-Raman and FT-IR spectroscopic study of synthetic Mg/Zn/Al-hydrotalcites. *Journal of Raman Spectroscopy, 35*(11), 967-974.

Kołodziejczak-Radzimska, A., & Jesionowski, T. (2014). Zinc oxide – from synthesis to application: a review. *Materials, 7*(4), 2833-2881. https://doi.org/10.3390/ma7042833

Kumar, P., Kumar, S., Tapwal, A., & Thakur, N. (2024a). Chemical/green synthesized cobalt/copper-doped α-Fe_2O_3 nanoparticles: potential for environmental remediation. *Journal of Materials Research, 39*(5), 836-849. https://doi.org/10.1557/s43578-023-01274-5

Kumar, P., Pathak, D. & Thakur, N. Trimetallic doped hematite (α-Fe2O3) (2024b). Nanoparticles using biomolecules of *Azadirachtaindica* leaf extract for photocatalytic dye removal: insights into catalyst stability and reusability. *Emergent Mater.* https://doi.org/10.1007/s42247-024-00742-w.

Kumar, P., Tapwal, A., Kumar, S., & Thakur, N. (2024c). Improved photocatalytic and free radical scavenging studies of synthesized polymer PVP/Azadirachtaindica leave extract-mediated Ni-Zn doped hematite nanoparticles. *Advances in Natural Sciences: Nanoscience and Nanotechnology, 15*(2), 025014. Doi: 10.1088/2043-6262/ad50bb

Kumar, P., Thakur, N., Kumar, K., Kumar, S., Dutt, A., Thakur, V. K., … & Thakur, N. (2024d). Catalyzing innovation: Exploring iron oxide nanoparticles-Origins, advancements, and future application horizons. *Coordination Chemistry Reviews, 507*, 215750. https://doi.org/10.1016/j.ccr.2024.215750

Madan, H. R., Sharma, S. C., Suresh, D., Vidya, Y. S., Nagabhushana, H., Rajanaik, H., … & Maiya, P. S. (2016). Facile green fabrication of nanostructure ZnO plates, bullets, flower, prismatic tip, closed pine cone: their antibacterial, antioxidant, photoluminescent and photocatalytic properties. *SpectrochimicaActa Part A: Molecular and Biomolecular Spectroscopy, 152*, 404-416. https://doi.org/10.1016/j.saa.2015.07.067

Mahendra, C., Murali, M., Manasa, G., Ponnamma, P., Abhilash, M. R., Lakshmeesha, T. R., … & Sudarshana, M. S. (2017). Antibacterial and antimitotic potential of bio-fabricated zinc oxide nanoparticles of Cochlospermumreligiosum (L.). *Microbial pathogenesis, 110*, 620-629. https://doi.org/10.1016/j.micpath.2017.07.051

Malaikozhundan, B., Vaseeharan, B., Vijayakumar, S., Pandiselvi, K., Kalanjiam, M. A. R., Murugan, K., & Benelli, G. (2017). Biological therapeutics of Pongamiapinnata coated zinc oxide nanoparticles against clinically important pathogenic bacteria, fungi and MCF-7 breast cancer cells. *Microbial Pathogenesis, 104*, 268-277. https://doi.org/10.1016/j.micpath.2017.01.029

Maslowsky Jr., E. (2019). *Vibrational spectra of organometallics: theoretical and experimental data.* John Wiley & Sons.

Mirza, A. U., Kareem, A., Nami, S. A., Bhat, S. A., Mohammad, A., & Nishat, N. (2019). Maluspumila and Juglenregia plant species mediated zinc oxide nanoparticles: synthesis, spectral

characterization, antioxidant and antibacterial studies. *Microbial Pathogenesis, 129*, 233-241. https://doi.org/10.1016/j.micpath.2019.02.020

Mobarak, M. B., Hossain, M. S., Yeasmin, Z., Mahmud, M., Rahman, M. M., Sultana, S., … & Ahmed, S. (2022). Probing the photocatalytic competency of hydroxyapatite synthesized by solid state and wet chemical precipitation method. *Journal of Molecular Structure, 1252*, 132142. https://doi.org/10.1016/j.molstruc.2021.132142

Pai, S., Sridevi, H., Varadavenkatesan, T., Vinayagam, R., & Selvaraj, R. (2019). Photocatalytic zinc oxide nanoparticles synthesis using Peltophorumpterocarpum leaf extract and their characterization. *Optik, 185*, 248-255. https://doi.org/10.1016/j.ijleo.2019.03.101

Prakasham, R. S., Kumar, B. S., Kumar, Y. S., & Kumar, K. P. (2014). Production and characterization of protein encapsulated silver nanoparticles by marine isolate Streptomyces parvulus SSNP11. *Indian Journal of Microbiology, 54*, 329-336. https://doi.org/10.1007/s12088-014-0452-1

Prasad, K. S., Prasad, S. K., Veerapur, R., Lamraoui, G., Prasad, A., Prasad, M. N., … & Shivamallu, C. (2021). Antitumor potential of green synthesized ZnONPs using root extract of Withaniasomnifera against human breast cancer cell line. *Separations, 8*(1), 8. https://doi.org/10.3390/separations8010008

Qidwai, A., Pandey, A., Kumar, R., Shukla, S. K., & Dikshit, A. (2018). Advances in biogenic nanoparticles and the mechanisms of antimicrobial effects. *Indian Journal of Pharmaceutical Sciences, 80*(4).

Rajabi, H. R., Naghiha, R., Kheirizadeh, M., Sadatfaraji, H., Mirzaei, A., & Alvand, Z. M. (2017). Microwave assisted extraction as an efficient approach for biosynthesis of zinc oxide nanoparticles: synthesis, characterization, and biological properties. *Materials Science and Engineering: C, 78*, 1109-1118. https://doi.org/10.1016/j.msec.2017.03.090

Rajendran, N. K., George, B. P., Houreld, N. N., & Abrahamse, H. (2021). Synthesis of zinc oxide nanoparticles using Rubusfairholmianus root extract and their activity against pathogenic bacteria. *Molecules, 26*(10), 3029. https://doi.org/10.3390/molecules26103029

Ramya, V., Kalaiselvi, V., Kannan, S. K., Shkir, M., Ghramh, H. A., Ahmad, Z., … & Vidhya, N. (2022). Facile synthesis and characterization of zinc oxide nanoparticles using Psidium guajava leaf extract and their antibacterial applications. *Arabian Journal for Science and Engineering, 47*(1), 909-918. https://doi.org/10.1007/s13369-021-05717-1

Rana, A., Kumar, P., Thakur, N., Kumar, S., Kumar, K., & Thakur, N. (2024). Investigation of photocatalytic, antibacterial and antioxidant properties of environmentally green synthesized zinc oxide and yttrium doped zinc oxide nanoparticles. *Nano-Structures & Nano-Objects, 38*, 101188. https://doi.org/10.1016/j.nanoso.2024.101188

Rehan, M., Ahmed-Farid, O. A., Ibrahim, S. R., Hassan, A. A., Abdelrazek, A. M., Khafaga, N. I., & Khattab, T. A. (2019). Green and sustainable encapsulation of Guava leaf extracts (Psidium guajava L.) into alginate/starch microcapsules for multifunctional finish over cotton gauze. *ACS Sustainable Chemistry & Engineering, 7*(22), 18612-18623. https://doi.org/10.1021/acs.iecr.4c01969

Ren, F., Xin, R., Ge, X., & Leng, Y. (2009). Characterization and structural analysis of zinc-substituted hydroxyapatites. *Actabiomaterialia, 5*(8), 3141-3149. https://doi.org/10.1016/j.actbio.2009.04.014

Rouhi, J., Mahmud, S., Naderi, N., Ooi, C. R., & Mahmood, M. R. (2013). Physical properties of fish gelatin-based bio-nanocomposite films incorporated with ZnOnanorods. *Nanoscale Research Letters, 8*, 1-6. https://doi.org/10.1186/1556-276X-8-364

Ruangtong, J., Jiraroj, T., & T-Thienprasert, N. P. (2020). Green synthesized ZnOnanosheets from banana peel extract possess anti-bacterial activity and anti-cancer activity. *Materials Today Communications, 24*, 101224. https://doi.org/10.1016/j.mtcomm.2020.101224

Saha, R., Subramani, K., Raju, S. A. K. P. M., Rangaraj, S., & Venkatachalam, R. (2018). Psidium guajava leaf extract-mediated synthesis of ZnO nanoparticles under different processing parameters for hydrophobic and antibacterial finishing over cotton fabrics. *Progress in Organic Coatings, 124*, 80-91. https://doi.org/10.1016/j.porgcoat.2018.08.004

Samat, N. A., & Nor, R. M. (2013). Sol-gel synthesis of zinc oxide nanoparticles using Citrus aurantifolia extracts. *Ceramics International, 39*, S545-S548. https://doi.org/10.1016/j.ceramint.2012.10.132

Sharma, S., & Kumar, K. (2021). Aloe-vera leaf extract as a green agent for the synthesis of CuO nanoparticles inactivating bacterial pathogens and dye. *Journal of Dispersion Science and Technology, 42*(13), 1950-1962. https://doi.org/10.1080/01932691.2020.1791719

Siddiqi, K. S., Husen, A., & Rao, R. A. (2018). A review on biosynthesis of silver nanoparticles and their biocidal properties. *Journal of Nanobiotechnology, 16*, 1-28. https://doi.org/10.1186/s12951-018-0334-5

Singhai, M., Chhabra, V., Kang, P., & Shah, D. O. (1997). Synthesis of ZnO nanoparticles for varistor application using Zn-substituted aerosol OT microemulsion. *Materials Research Bulletin, 32*(2), 239-247. https://doi.org/10.1016/S0025-5408(96)00175-4

Song, J. Y., & Kim, B. S. (2008). Biological synthesis of bimetallic Au/Ag nanoparticles using Persimmon (Diopyros kaki) leaf extract. *Korean Journal of Chemical Engineering, 25*, 808-811. https://doi.org/10.1007/s11814-008-0133-z

Sukri, S. N. A. M., Shameli, K., Wong, M. M. T., Teow, S. Y., Chew, J., & Ismail, N. A. (2019). Cytotoxicity and antibacterial activities of plant-mediated synthesized zinc oxide (ZnO) nanoparticles using Punicagranatum (pomegranate) fruit peels extract. *Journal of Molecular Structure, 1189*, 57-65. https://doi.org/10.1016/j.molstruc.2019.04.026

Sun, J. H., Dong, S. Y., Feng, J. L., Yin, X. J., & Zhao, X. C. (2011). Enhanced sunlight photocatalytic performance of Sn-doped ZnO for Methylene Blue degradation. *Journal of Molecular Catalysis A: Chemical, 335*(1-2), 145-150. https://doi.org/10.1016/j.molcata.2010.11.026

Thakur, N., & Thakur, N. (2024a). Degradation of textiles dyes and scavenging activity of spherical shape obtained anatase phase of Co-Ni-doped TiO2 nanocatalyst. *Journal of Materials Science: Materials in Electronics, 35*(2), 134. https://doi.org/10.1007/s10854-023-11851-3

Thakur, N., & Thakur, N. (2024b). Photocatalytic adsorption and scavenging potential of chemical and green encapsulated anatase phase of coupled doped Zn-Co TiO2 nanoparticles. *Journal of Dispersion Science and Technology*, 1-16. https://doi.org/10.1080/01932691.2024.2312841

Thakur, N., Thakur, N., Kumar, A., Thakur, V. K., Kalia, S., Arya, V., … & Kyzas, G. Z. (2024c). A critical review on the recent trends of photocatalytic, antibacterial, antioxidant and nanohybrid applications of anatase and rutile TiO2 nanoparticles. *Science of The Total Environment*, 169815. https://doi.org/10.1016/j.scitotenv.2023.169815

Thakur, S., Kumar, P., Thakur, N., Kumar, K., Jeet, K., Kumar, S., & Thakur, N. (2024d). Photocatalytic, antibacterial and antioxidant potential of spheroidal shape chromium and yttrium doped cobalt oxide nanoparticles: A green approach. *Journal of the Indian Chemical Society*, 101199. https://doi.org/10.1016/j.jics.2024.101199

Thakur, N., Kumar, A., & Thakur, N. (2023). Tinosporacordifolia and polyvinylpyrrolidone encapsulated dual doped Ni-Cu TiO2 emerging nanocatalyst for the removal of organic dyes from wastewater and its free radical assay activity. *Hybrid Advances, 4*, 100086. https://doi.org/10.1016/j.hybadv.2023.100086

Verma, N., Pathak, D., & Thakur, N. (2024). Eco-friendly green synthesis of (Cu, Ce) dual-doped ZnO nanoparticles with Colocasia esculenta plant extract using microwave assisted technique for antioxidant and antibacterial activity. *Next Materials, 5*, 100271. https://doi.org/10.1016/j.nxmate.2024.100271

Vijayakumar, S., Vaseeharan, B., Malaikozhundan, B., & Shobiya, M. (2016). Laurusnobilis leaf extract mediated green synthesis of ZnO nanoparticles: Characterization and biomedical applications. *Biomedicine & Pharmacotherapy, 84*, 1213-1222. https://doi.org/10.1016/j.biopha.2016.10.038

Zare, E., Pourseyedi, S., Khatami, M., & Darezereshki, E. (2017). Simple biosynthesis of zinc oxide nanoparticles using nature's source, and it's in vitro bio-activity. *Journal of Molecular Structure, 1146*, 96-103. https://doi.org/10.1016/j.molstruc.2017.05.118

Zhang, L., Gu, F. X., Chan, J. M., Wang, A. Z., Langer, R. S., & Farokhzad, O. C. (2008). Nanoparticles in medicine: therapeutic applications and developments. *Clinical Pharmacology & Therapeutics, 83*(5), 761-769. https://doi.org/10.1038/sj.clpt.6100400